HHS Public Access

Author manuscript

J Control Release. Author manuscript; available in PMC 2018 June 10.

Published in final edited form as:

J Control Release. 2017 June 10; 255: 108–119. doi:10.1016/j.jconrel.2017.04.016.

Targeted drug distribution in tumor extracellular fluid of GD2-expressing neuroblastoma patient-derived xenografts using SN-38-loaded nanoparticles conjugated to the monoclonal antibody 3F8

Carles Monterrubio[a,b], **Sonia Paco**[a,b,1], **Nagore G. Olaciregui**[a,b,1], **Guillem Pascual-Pasto**[a,b], **Monica Vila-Ubach**[a,b], **Maria Cuadrado-Vilanova**[a,b], **M. Mar Ferrandiz**[a,b], **Helena Castillo-Ecija**[a,b], **Romina Glisoni**[c], **Nataliya Kuplennik**[d], **Achim Jungbluth**[e], **Carmen de Torres**[a,b], **Cinzia Lavarino**[a,b], **Nai-Kong V. Cheung**[e], **Jaume Mora**[a,b], **Alejandro Sosnik**[d,f], and **Angel M. Carcaboso**[a,b,*]

[a]Institut de Recerca Sant Joan de Deu, 08950 Barcelona, Spain

[b]Department of Pediatric Hematology and Oncology, Hospital Sant Joan de Deu, 08950 Barcelona, Spain

[c]CONICET-Department of Pharmaceutical Technology, Faculty of Pharmacy and Biochemistry, Universidad de Buenos Aires, CP1113 Buenos Aires, Argentina

[d]Laboratory of Pharmaceutical Nanomaterials Science, Department of Materials Science and Engineering, Technion-Israel Institute of Technology, 3200003 Haifa, Israel

[e]Memorial Sloan-Kettering Cancer Center, New York, NY 10021, USA

[f]Russell Berrie Nanotechnology Institute (RBNI), Technion-Israel Institute of Technology, 3200003 Haifa, Israel

Abstract

Neuroblastoma is a pediatric solid tumor with high expression of the tumor associated antigen disialoganglioside GD2. Despite initial response to induction therapy, nearly 50% of high-risk neuroblastomas recur because of chemoresistance. Here we encapsulated the topoisomerase-I inhibitor SN-38 in polymeric nanoparticles (NPs) surface-decorated with the anti-GD2 mouse mAb 3F8 at a mean density of seven antibody molecules per NP. The accumulation of drug-loaded NPs targeted with 3F8 versus with control antibody was monitored by microdialysis in patient-derived GD2-expressing neuroblastoma xenografts. We showed that the extent of tumor penetration by SN-38 was significantly higher in mice receiving the targeted nano-drug delivery system when compared to non-targeted system or free drug. This selective penetration of the

*Correspondence: amontero@fsjd.org (A.M. Carcaboso); Tel: +34 936009751 EXT 4420; Fax: +34 936009771.
[1]These authors contributed equally to this work

tumor extracellular fluid translated into a strong anti-tumor effect prolonging survival of mice bearing GD2-high neuroblastomas *in vivo*.

Graphical Abstract

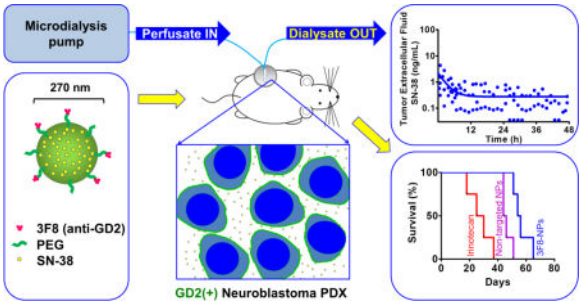

Keywords

GD2-targeted nanoparticles; intratumor drug distribution; microdialysis; tumor extracellular fluid; neuroblastoma; irinotecan/SN-38; PDX models

Introduction

Intensive systemic chemotherapy has significantly improved overall survival from cancer - a leading cause of death among infants in Europe and in the USA - over the last 30 years [1]. However, children with metastatic solid tumors often develop recurrence because of drug resistance, not easily overcome by increasing dose or intensity despite pushing the limits of acute and late toxicities [2]. Among the difficult-to-cure pediatric cancers, high-risk neuroblastoma is the most frequent extracranial solid tumor in patients under 5 years of age, and nearly 50% of stage 4 disease is incurable [3].

Among the more recently tested chemotherapies for relapsed or refractory neuroblastoma, the topoisomerase I inhibitor irinotecan represents a prodrug which is converted *in vivo* to the active metabolite SN-38 [4, 5]. The clinical application of irinotecan, however, has not fulfilled its expectations in high-risk neuroblastoma [6]. A plausible reason for this poor performance is the insufficient conversion to SN-38 because of the reduced activity of human carboxylesterases when compared to murine models [7]. It has been estimated that irinotecan conversion to SN-38 is only 5% in humans [8], versus 70% in mice [9].

To achieve the full benefit from drug exposure, SN-38 has been formulated in several drug delivery systems (DDS) [10]. We recently observed that local SN-38 delivery in the surgical bed maximizes exposure to the drug in neuroblastoma patient-derived xenografts (PDX) and achieves improved local tumor control in highly chemoresistant pediatric tumor models, when compared to equimolar irinotecan [11]. Similarly, novel formulations of SN-38 prodrugs designed for intravenous (i.v.) administration showed higher efficacy in neuroblastoma xenografts [12, 13]. In other cancers, SN-38-loaded self-assembly nanoparticles (NPs) have consistently outperformed irinotecan [14]. All things considered, the ability to maintain a size of the NPs to less than 300 nm can increase drug penetration in

tumors by passive extravasation and drug retention (through the EPR effect) [15] accounting for the improved safety/activity profile of these nano-DDS.

However, these strategies reported to date still lack selectivity, complicated by innocent bystander damage and limited efficacy when applied to patients. To improve selectivity, antibody-based targeting strategies directed at the disialoganglioside GD2 seem obvious [16–18]. GD2 is expressed in pediatric solid tumors including neuroblastoma, Ewing sarcoma, rhabdomyosarcoma, osteosarcoma and retinoblastoma [16, 19]. Almost all stroma-poor high-risk neuroblastomas express GD2 ubiquitously [20], while GD2 expression is restricted in normal tissues. High-risk neuroblastoma patients treated with monoclonal anti-GD2 antibodies have been cured with no long late effects in their GD2(+) normal organs, which included neurons, pain fibers and basal layers of the skin [21, 22]. The anti-GD2 chimeric (human-mouse) ch14.18 antibody (Unituxin™) has proven efficacy on overall survival in a randomized trial among high risk patients treated in first remission [22], while murine 3F8 has also shown highly favorable long term cure rates over the last 3 decades [3]. The clinical utility of antibodies targeting GD2 was recently summarized [23].

The commercial availability of anti-GD2 antibodies has stimulated the development of GD2-targeted systems for neuroblastoma therapy or diagnosis [24–27]. Using *in vivo* imaging, GD2-targeted formulations are shown to accumulate in GD2-expressing xenografts to a greater extend and with more selectivity than the non-targeted ones [25–27]. However, the pharmacokinetics of specific drugs loaded into GD2-targeted products has not been well characterized. Specifically, it has not been assessed whether such systems induce higher or more prolonged exposure of drugs in the tumor extracellular fluid (tECF), as compared to other non-targeted control systems. Furthermore, to preserve the heterogeneity of real human tumors, PDX models that resemble better the anatomy and genetics of the fresh tumor sample, as compared to xenografts derived from cell lines, have not been exploited in previous studies [28]. Such models have become preferred *in vivo* tools in strategies for anti-cancer nanomedicine development [29].

We hypothesized that SN-38-loaded polymeric NPs conjugated to 3F8 would lead to increased specific accumulation of the actively targeted drug SN-38 in the tECF of PDX models. Here we have developed such NPs, characterized their *in vitro* biochemical properties and their specific ability to target GD2-expressing neuroblastoma cells *in vitro* and PDX models *in vivo*. To assess the intratumoral pharmacokinetics of SN-38 we used microdialysis, a technique that enables the quantification of the drug in the extracellular fluids of tissues in the same animal over time [30, 31]. The efficacy of this platform was demonstrated using a GD2-expressing PDX neuroblastoma model.

Materials and Methods

Materials

SN-38 was obtained from Seqchem (Pangbourne, UK). Irinotecan for *in vivo* studies was purchased from Hospira (Lake City, IL). Clinical grade mouse monoclonal antibody (mAb) 3F8 was made under the supervision of Dr. Nai-Kong V. Cheung at Memorial Sloan Kettering Cancer Center (MSKCC, New York, NY) [19]. Murine IgG3 (purified

immunoglobulin from murine myeloma, clone DX), bovine serum albumin (BSA), 2-hydroxypropyl-β-cyclodextrin (HPBCD), polyvinyl alcohol (PVA, weight-molecular weight (M_w) 30–70 kDa), 2-(*N*-morpholino)ethanesulfonic acid (MES) buffer, 1-ethyl-3-(3-dimethylaminopropyl)carbodiimide hydrochloride (EDC), *N*-hydroxysulfosuccinimide (NHS), 3,6-dimethyl-1,4-dioxane-2,5-dione (D,L-lactide), tin(II) octanoate, anhydrous acetate, phosphate buffered saline (PBS) tablets, sodium hydroxide (NaOH) and dimethyl sulfoxide (DMSO) were purchased from Sigma-Aldrich (St. Louis, MO). Tetrahydrofuran (THF) was from Chen Samuel Chemicals (Haifa, Israel). Glacial acetic acid, triethylamine (TEA), ethyl acetate (EtOAc), di-sodium tetra-borate 10-hydrate and *N,N*-dimethylformamide (DMF) were from Panreac (Barcelona, Spain). Water was from Milli-Q water purification system (Millipore, Bedford, MA). Heterobifunctional carboxymethyl-polyethylene glycol (HO-PEG-COOH, M_w 3.4 kg/mole) was from Laysanbio (Arab, AL). Reagents for cell culture were from Life Technologies (Grand Island, NY).

Preparation of SN-38-loaded NPs

NPs were prepared by a single oil-in-water emulsion method [32]. To produce NPs that display reactive functional groups on the surface for the conjugation of the different ligands, the NP matrix was composed of a mixture of acid-terminated poly(lactic-co-glycolic acid) (PLGA; M_w of 7–17 kg/mole, Evonik Industries AG Co., Essen, Germany) (95% w/w) and carboxymethyl-poly(ethylene glycol)-*b*-poly(lactic acid) (PLA-PEG-COOH) (5% w/w). PLA-PEG-COOH was synthetized by the ring-opening polymerization of D,L-lactide by the terminal -OH moieties of HO-PEG-COOH in presence of tin(II) octanoate as catalyst at 145 °;C under magnetic stirring (2.5 h). The feeding ratio was tuned to obtain a copolymer with M_w of approximately 15 kg/mole. M_w, number-molecular weight (M_n), and dispersity index [Đ (M_w/M_n)] of the PLA-PEG-COOH copolymer were characterized by Gel Permeation Chromatography (GPC; Alliance HPLC system, Waters, Milford, MA) using a refractive index detector and 4 Styragel HR (1–4) columns (7.8 × 300 mm, packed with 5 μm particles, Waters). Previous to injection, samples were dissolved in THF at a concentration of 1 % (w/v) and filtered through 0.45 μm filters. Runs were conducted at a flow rate of 1 mL/min, at 40°C.

For the preparation of 200 mg batches of the reference NPs (R-NPs), 9 mg PLA-PEG-COOH was dissolved in 3.6 mL ethyl acetate and added to 171 mg of PLGA powder. Alternatively, in preliminary optimization experiments, the proportion of PLA-PEG-COOH was increased to 10% and 20% w/w. Each of the polymer blend solutions (3.6 mL) was then added to 3.6 mL DMSO containing 20 mg SN-38 (to achieve 10% theoretical load in the final formulation). Blank NPs (without SN-38) were manufactured following the same protocol though without the addition of the drug. The resulting mixture was added to 20 mL of PVA 1% w/v in water and sonicated for 30 s (2 s on – 1 s off cycles) in an ice bath. The oil-in-water emulsion was immediately added to 240 mL of acetate buffer (pH = 4.8) and stirred for 24 h away from light for solvent diffusion and evaporation. The dispersion of hardened NPs was then centrifuged in 25 mL tubes for 1 h at 60,000 *g*. R-NPs pellets were washed twice with water to remove PVA, followed by 30 min 60,000 *g* centrifugation after each wash. The final pellet was dispersed in 10 mL water containing HPBCD (100 mg) as cryo-protectant [33], frozen in liquid nitrogen and freeze-dried.

To produce NPs conjugated to the anti-GD2 mouse mAb 3F8 (3F8-NPs; 100 mg), we followed the same protocol until the first wash of the hardened R-NPs. Then, the pellet was resuspended in 20 mL MES buffer 0.01 M (pH 5.5) together with 1 mL of NHS and 0.5 mL of EDC, as previously described [34]. EDC and NHS were used to activate the carboxyl groups of PLA-PEG-COOH on the NP surface and form an intermediate that can react with primary amine groups in the side-chain of the antibodies [34]. This solution was stirred for 15 min and washed with 200 mL of MES buffer, followed by 30 min centrifugation at 60,000 *g*. The pellet was then resuspended in 16 mL PBS 10x, and 3.5 mL MES buffer and 500 μL (100 μg) of 3F8 murine mAb in MES buffer were added to the suspension of activated NPs. The mixture containing the antibody and the activated NPs was stirred for 3 h away from light. Three final washes with water and alternating centrifugation were performed to remove the excess of antibody (remaining in the supernatant), MES buffer and PBS. Finally, the pellet was resuspended in 5 mL of water containing 50 mg of HPBCD, frozen and freeze-dried for 72 h. Additionally, NPs conjugated with murine IgG3 (IgG3-NPs; same subclass as 3F8 antibody) were manufactured as control NPs.

Characterization of the NPs

Particle size (z-average), polydispersity index (PDI) and zeta-potential were determined in a Zetasizer Nano ZS from Malvern Instruments (Malvern, UK). The morphology of the NPs was visualized by high resolution-scanning electron microscopy (HR-SEM; Zeiss Ultra-Plus FEG-SEM, Cambridge, MA). NP counts were performed by Nanoparticle Tracking Analysis (NTA, NanoSight NS500-Zeta HSB 41 system with high sensitivity camera and 638 nm laser for fluorescent analysis, Malvern Instruments). The efficiency of the antibody conjugation was calculated by ELISA quantification of the non-conjugated antibody fraction in the supernatant after the 15 min EDC/NHS reaction. For the ELISA, goat anti-mouse IgG-coated 96 well plates (Life Technologies) were blocked with 5% BSA in PBS for 1 h, supernatants were plated and incubated overnight. The secondary antibody was a goat anti-mouse IgG, peroxidase conjugate (Promega, Fitchburg, WI).

To calculate the amount of 3F8 antibodies conjugated per NP, we considered the conjugation efficiency-corrected proportion of antibody:NP in the reaction. We applied the Avogadro number to calculate the number of conjugated molecules of antibody in a given count of NPs. We considered 150 kDa as the molecular weight of 3F8 [35].

SN-38 load in NPs was quantified upon hydrolysis of the polymers in NaOH 0.1 M. To produce working solutions for the calibration curve, SN-38 (stock in DMSO) was diluted in NaOH 0.1 M containing hydrolyzed blank NPs (without drug). Appropriate volumes of the working solutions were added to pH 7.4 PBS containing 10% HPBCD (w/v) to build the final calibration curve. HPLC analysis of SN-38 was performed as previously described [31].

SN-38 release from NPs

To determine the release profile of SN-38 from the mAb-modified NPs, samples containing 100 μg of encapsulated SN-38 were resuspended in 3 mL of pH 7.4 PBS (10% HPBCD) and loaded into a 40 kDa cutoff Slide-A-Lyzer G2 dialysis cassettes from Thermo Fisher

(Waltham, MA). The cassettes were placed individually in hermetic plastic bags with 10 mL of pH 7.4 PBS (10% HPBCD), at 37 °C, in continuous stirring for 96 h. At sampling times 0.5, 1, 2, 4, 6, 8, 12, 24, 48, 72, 96 h, buffer from the airtight plastic bags was completely removed and replaced with fresh buffer. Then, 100 μL of the removed buffer was processed as previously described to analyze SN-38 [31]. The rate of drug release was analyzed by fitting the data into first order equation(1),

$$\ln(100 - Q) = \ln 100 - \mathrm{kt} \quad (1)$$

where Q is the percentage of SN-38 released at time t, and k is the release rate constant.

Tumor models

Neuroblastoma cell lines LAN-1 (kindly provided by Dr. Robert Seeger at CHLA), SK-N-JD and SK-N-LP (from Dr. Nai-Kong V. Cheung of MSKCC), and SK-N-AS, IMR-5, SH-EP1 and SH-SY5Y (ATCC), and HeLa cell line (ovarian carcinoma; ATCC), were maintained in the repository at Hospital Sant Joan de Deu (HSJD, Barcelona) and cultured as previously described [31]. Neuroblastoma, Ewing sarcoma and rhabdomyosarcoma PDX models were established from patient biopsies at HSJD under an Institutional Review Board-approved protocol. Neuroblastoma PDX models HSJD-NB-007 and HSJD-NB-011 were derived from patients refractory to all treatments (including irinotecan) and were used for the *in vivo* studies. HSJD-NB-007 was established from a 5 year old male with progressive stage 4 disease, amplification of *MYCN* gene and no mutations in *TP53* and *ALK*. HSJD-NB-011 was from a 2.5 year old male with progressive stage 4 disease, amplification of *MYCN* gene, *TP53* wild type and *ALK*-mutated (I1171N). For *in vivo* studies, fresh tumor fragments (25–50 mm^3) were subcutaneously transplanted to the flank of nude mice (Envigo, Barcelona, Spain). The research conducted with mice adhered to the European regulations and it was approved by the local animal care and use committee (135/11).

Expression of GD2 in tumor models

Selected tumor models were characterized for GD2 antigen expression in cultured cells by an immunofluorescence method already described [36]. All models were analyzed for relative mRNA expression of *GD2 synthase* [beta-1,4-N-acetyl-galactosaminyl transferase (GalNAc-T)] by real-time quantitative PCR (RT-qPCR), as previously described [36]. The expression of the GD2 antigen in selected PDX models was further studied by immunohistochemistry (IHC) in formalin-fixed paraffin-embedded tissue sections as previously described [37].

In vitro binding of 3F8 to GD2

To determine whether the 3F8 mAb was still able to target GD2 upon conjugation to NPs, a competitive binding immunofluorescence assay was performed. The surface of 8-well EMD Millipore Millicell EZ Slides (Millipore) was coated with 100,000 LAN-1 (GD2(+)) or HeLa (GD2(−)) cells in culture. After 24 h at 37°C and 5% CO_2, the medium was removed, cells were fixed in paraformaldehyde (4%) for 15 min at 4°C, washed 3 times (PBS-Tween 0.05%) and blocked with BSA (3% in PBS) for 1 h. Then, either IgG3-NPs (10,000 μg/mL)

or 3F8-NPs (0, 1, 10, 100, 1000 and 10,000 μg/mL) suspended in fresh culture medium were added to the wells, in triplicate, and incubated for 1 h, at room temperature (RT). Consecutively, a fixed amount of free 3F8 (5 μg in 500 μL) was added to the wells and incubated for 1 h to compete for free GD2 antigens on the cells surface. After 3 washes, wells were incubated with FITC-labeled secondary rabbit anti-mouse antibody (1:5000) and 4′ 6-diamidino-2-phenylindole (DAPI; to stain nuclei) for 1 h, at RT. Finally, fluorescence microscopy pictures were obtained (Leica DM 5000 B, Wetzlar, Germany) and quantified with ImageJ (NIH, Bethesda, MD).

In vitro activity of NPs

To study the antiproliferative activity of SN-38, either free (from a stock in DMSO) or carried by R-NPs, IgG3-NPs or 3F8-NPs, 10,000 LAN-1 or HeLa cells were plated in 96-well plates, cultured overnight, and treated with serial dilutions of each formulation. The MTS assay (Promega) was used to determine cell viability after 72 h of incubation. The concentrations of drug required to cause a reduction of 50% in cell proliferation (IC50 and 95% confidence intervals) were calculated with Graphpad Prism 5 software (La Jolla, CA).

Similarly, a time-course experiment was performed on LAN-1 cells, washing the SN-38 products out of the culture medium at time points 4, 8 and 24 h.

The activity of the NPs was also studied in primary cultures from freshly excised PDX tissues established by disaggregation with collagenase-DNase enzymes (Sigma-Aldrich). In these experiments, 50,000 cells were plated and the antiproliferative activity of the products was assayed after overnight culture [11].

Pharmacokinetics of SN-38 in mice with neuroblastoma

To characterize plasma concentration-time profiles of lactone SN-38 after i.v. administration of each formulation, 62 nude mice bearing HSJD-NB-007 tumors received one i.v. dose of 4 mg/kg SN-38 in NPs (IgG3-NPs or 3F8-NPs). As reference, a group of mice received 10 mg/kg irinotecan i.v. (equimolar SN-38 dose upon i.v. irinotecan metabolization to SN-38 in mice) [9]. Plasma samples were obtained at different time points until 24 h and total lactone SN-38 was quantified after protein precipitation in cold methanol, as described previously [31]. In mice receiving irinotecan, such total SN-38 concentration was the sum of the plasma protein-bound and unbound fractions. In this group, the unbound plasma SN-38 concentration was calculated by the application of the plasma protein binding factor (81.4%) calculated in a previous work by the ultrafiltration method [31]. In mice receiving NPs, total SN-38 concentration was the sum of the fraction still encapsulated in the NPs and the fraction already released from NPs (either bound or unbound to proteins). In these two groups, one aliquot of each plasma sample was processed also as ultrafiltrate to determine the free fraction (protein unbound) of the released SN-38. Total (bound + unbound) released SN-38 was calculated upon the application of the protein binding factor to the ultrafiltrate (81.4%). The maximum concentration achieved in plasma (C_{max}) was calculated by extrapolation at time 0 of the initial fast exponential decay curve.

Long-term delivery of SN-38 in tECF was studied *in vivo* in tumor-bearing mice using intratumoral microdialysis [11, 31]. Briefly, 20 kDa cutoff, 4 mm-length microdialysis

probes (CMA, Kista, Sweden) were inserted into subcutaneous HSJD-NB-007 tumors implanted in 13 mice under isoflurane anesthesia, and fixed with sutures to the skin. PBS with HPBCD 10% (w/v) was used as perfusion fluid at a flow rate of 0.5 μL/min. After 90 min equilibration, mice received either irinotecan 10 mg/kg, or SN-38 4 mg/kg in IgG3-NPs or 3F8-NPs, and 1.5 h dialysate samples (45 μL) were collected serially in a CMA 470 refrigerated fraction collector (CMA, Kista, Sweden) as previously described, and stored at −80 °C until HPLC analysis using a published method [31].

Microdialysis probes were calibrated using the mean recovery value (70%) previously determined *in vivo* at steady state SN-38 plasma levels [31]. Areas under the concentration-time curves (AUC) of unbound SN-38 in plasma and tECF dialysates were calculated with the trapezoid method. The standard error of the calculated plasma AUC was calculated with the law of propagation of errors as previously described [38]. The terminal elimination half-life in plasma was calculated by linear regression of the log(concentration) versus time data of the final concentration-time curve.

In vivo activity of NPs

For activity assays in mice, we selected the PDXs HSJD-NB-007 and HSJD-NB-011 as models with intense and weak expression of *GD2 synthase*, respectively (see RT-qPCR Results). Freshly excised tumors from one mouse bearing the third generation of each PDX were fragmented and implanted subcutaneously in nude mice. When the tumors reached 100–300 mm^3, mice were treated with either irinotecan 10 mg/kg [5 days per week for 2 consecutive weeks, or (dx5)x2] [4], irinotecan 10 mg/kg [on days 1 and 4 of the week for 3 weeks, or (q3d)x3], SN-38 4 mg/kg in IgG3-NPs (q3d)x3, or SN-38 4 mg/kg in 3F8-NPs (q3d)x3. The regimen of irinotecan 10 mg/kg (dx5)x2 has been previously shown active against neuroblastoma [4], while the SN-38 (q3d)x3 regimens administered to the other groups reduced the total dose received in the (dx5)x2 regimen by 40%. Control mice were treated with saline following the (q3d)x3 schedule.

Tumor growth was measured with an electronic caliper. At the end of treatment [day 21, or day 14 for mice receiving (dx5)x2 irinotecan], response to treatment was evaluated according to standard criteria [39]. We defined complete response (CR) as tumor volume < 50 mm^3 and > 50% of tumor volume reduction; partial response (PR) was tumor volume regression ≥ 50% but total tumor volume ≥ 50 mm^3; stable disease (SD) was < 50% regression and ≤ 25% increase from initial volume; and progressive disease (PD) was > 25% increase from initial volume. Mice were euthanized when tumors reached 2000 mm^3.

Statistics

GraphPad Prism 5 was used to perform the statistical analyses. One-way ANOVA test using the Bonferroni's post-test to compare multiple groups was used to determine the differences in the mean tECF and plasma AUCs and tECF AUC-to-plasma ratios between treatments. For comparison of multiple survival curves, median survivals (calculated by the Kaplan-Meier method) were compared with the log-rank test with Bonferroni-corrected threshold.

Results

Development of GD2-targeted, SN-38-loaded NPs

Our first goal was to develop drug-loaded NPs using a reproducible method. In preliminary studies, we established the feasibility to load 10% w/w of SN-38 in PLGA NPs by the single emulsion technique. To provide a chemically reactive surface for the conjugation of antibodies under mild conditions that do not jeopardize the integrity of the cargo, we synthesized PLA-PEG-COOH block copolymer (Mn = 8.0 kg/mole; M_w = 13.2 kg/mole; Đ = 1.64, as determined by GPC). This copolymer was incorporated to a commercially available PLGA (M_w = 17 kg/mole) to produce the NPs. PEG blocks were expected to be accommodated at the water-organic solvent interphase of the droplets in the oil-in-water simple emulsion and thus, to ensure the availability of the reactive carboxylic acid moieties at the surface of the formed NPs to enable the subsequent conjugation of the antibody. This approach enables the fine tuning of the PEG concentration. When the proportion of PLA-PEG-COOH was set at 5% w/w, the encapsulation efficiency of SN-38 was >83% (Table 1). Conversely, higher concentrations (10–20% w/w) made the emulsion unstable and led to the crystallization of pure SN-38 and the uncontrolled precipitation of copolymer (data not shown). In the following step, the corresponding mAb was conjugated to the surface of the NPs using EDC/NHS chemistry. Table 1 summarizes the properties of the NP products, including the particle count by NTA.

Dynamic light scattering (DLS) analysis demonstrated that, regardless of the conjugation of the mAb, the mean size of all the NPs was below 300 nm (Table 1). These results were supported by HR-SEM that showed the spherical morphology of all the NPs and the change of the surface topography from a very smooth for R-NPs to a patterned one for IgG3-NPs and 3F8-NPs (Figure 1). In the latter two, the conjugated antibodies were visualized as small dots (<20 nm), as previously reported upon the conjugation of other proteins to polymeric NPs [40] and in line with the reported size of IgG antibodies [41]. Upon analysis of the non-conjugated fraction of antibody in the supernatant of the reaction, the calculated efficiency of the conjugation process was 96.7 ± 3.0%, i.e., most of the antibody reacted with the NPs in the selected conditions. As a result, each NP contained around 7 molecules of antibody (Table 1).

The zeta-potential of all the NPs was highly negative, a characteristic of PLA and PLGA NPs, though upon mAb conjugation, a slight increase to less negative values was observed due to the partial disappearance of terminal carboxylic acid groups and the positive charge of 3F8 antibodies [42] (Table 1).

To confirm the release of SN-38 from the NPs, a step that is critical for the antitumor activity, the kinetics was assessed *in vitro*. SN-38 is a very hydrophobic molecule, crystallizing in contact with water and undergoing significant adsorption to different surfaces (e.g., plastic tubing, glass vials) [31]. In this context, we included HPBCD as solubilizer (10% w/v) in the release medium. We observed identical release profile from IgG3-NPs and 3F8-NPs, with no burst effect, lag time of 2 h (in which they released 2.1 ± 0.8% and 1.9 ± 0.5%, respectively) and first-order release kinetics (r^2 of 0.97 and 0.99,

respectively; calculated with Graphpad Prism 5) that achieved the plateau at 48 h and released the complete load within 72 h (Figure 2).

Expression of the tumor antigen GD2 in models of pediatric solid tumors

LAN-1 and HeLa cells were selected as GD2(+) and GD2(−) tumor models, respectively [43, 44]. We confirmed the expression of GD2 in LAN-1 by immunofluorescence (Figure 3A). Then, we quantified the expression of *GD2 synthase* in both cell lines and in a series of neuroblastoma cell lines and pediatric PDX models established at our institution including seven neuroblastomas, six Ewing sarcomas and three rhabdomyosarcomas (two of them alveolar) by RT-qPCR (Figure 3B).

The expression of mRNA was normalized to the one of the LAN-1 ne/uroblastoma cell line and it was in the range 0.39–2.24 in the neuroblastoma cell lines. Neuroblastoma PDXs expressed the gene as well, although showed more variability among models (range 0.16–3.96). *GD2 synthase* expression was low or absent in Ewing sarcomas and rhabdomyosarcoma PDXs. Because adherent cultures of primary PDX models are difficult to maintain [45], we selected the LAN-1 and HeLa cell lines for further *in vitro* studies in adherent conditions. For *in vivo* assays we selected HSJD-NB-007 (GD2-high; 4.0-fold *GD2 synthase* expression as compared to LAN-1) and HSJD-NB-011 (GD2-low; 0.16-fold *GD2 synthase* expression as compared to LAN-1). Cells with GD2-positive cytoplasmic staining were found in FFPE sections of both models (Figure 3C), while rhabdomyosarcomas and Ewing sarcoma PDX were negative for GD2 staining.

Stability of 3F8 conjugated in NPs

Because the chemical modification might destroy immunoreactivity of the antibody, we performed a competitive binding assay in compartmentalized glass microscope slides coated with GD2(+) LAN-1 cells (Figure 4). We observed that increasing concentrations of 3F8-NPs added to the LAN-1 cells, from 1 μg/mL (Figure 4A) to 1000 μg/mL (Figure 4B), saturated the GD2 binding sites competing out the fluorescent labeling with soluble 3F8 in a dose-response fashion (Figure 4C). This binding of 3F8-NPs NPs was specific since exposing LAN-1 cells to high concentration of IgG3-NPs (10,000 μg/mL) did not block GD2 sites (Figure 4D). Thus, it was concluded that 3F8 antibody conserved a significant proportion of its selectivity and affinity for GD2 upon chemical conjugation.

Antiproliferative activity of NPs in culture

All the SN-38-loaded NPs retained activity in the low nanomolar concentration range (Figure 5A). Encapsulation resulted in a slight decrease of the IC50 (mean and 95% confidence intervals) from 5.8 (3.8–8.8) nM for free SN-38 to 1.7 (0.65–4.2), 0.77 (0.33–1.8) and 2.7 (1.4–5.2) for R-NPs, IgG3-NPs and 3F8-NPs, respectively. We confirmed that the IC50 of the free 3F8 antibody in GD2-expressing cells LAN-1 was 1.6 μg/mL (range 0.96–2.5) and >100 fold higher for GD2(−) cells (HeLa) (Figure 5B). In the time-course experiment on LAN-1 cells we did not find a time-dependent effect of the activity of the products at concentrations 100, 10 and 1 nM (Figure 5C). Primary cultures from PDX models HSJD-NB-007 and HSJD-NB-011 grew as aggregated clusters or tumorspheres and

were sensitive to SN-38 products in the nanomolar range. The activity of free SN-38 at 500 nM was significantly higher as compared to the one of the NP products (Figure 5D).

Distribution of SN-38 in plasma and tumor (tECF) in neuroblastoma

The subcutaneous PDX model HSJD-NB-007 (GD2-high) was used for drug distribution studies. Mice received either i.v. administration of 10 mg/kg irinotecan, the water soluble prodrug of SN-38, or equimolar doses of 4 mg/kg SN-38 encapsulated in IgG3-NPs or in 3F8-NPs. The inclusion of IgG3-NPs was to control for nonspecific targeting (produced by the EPR effect *in vivo* or by nonspecific antibody binding). Plasma SN-38 concentration-time curves are shown in Figure 6A.

The total amount of SN-38 in plasma of mice receiving NPs was a combination of SN-38 encapsulated in the NPs and SN-38 released from the NPs (either bound or unbound to proteins). After ultrafiltration, the unbound SN-38 in the released fraction could be quantified; the extrapolated peak of SN-38 (C_{max}) was 28.4, 53.3 and 30.0 ng/mL for free irinotecan, IgG3-NPs and 3F8-NPs groups, respectively. The half-life of SN-38 in the terminal elimination phase was greater for the NP formulations (3.8 h and 5.3 h for IgG3-NPs and 3F8-NPs, respectively), as compared to irinotecan (2.1 h), which could be due to sustained release of SN-38 from circulating NPs. Similar pharmacokinetics was reported for other SN-38 DDS [14].

Upon recovery-corrected analysis of tumor dialysates from microdialysis experiments (3–5 individual experiments per condition), concentration-time curves of unbound SN-38 in the tECF of mice were constructed (Figure 6B). In 5 out of 5 experiments, SN-38 was below the limit of quantification in tECF after 15 h of a single injection of i.v. irinotecan. Mice receiving IgG3-NPs showed longer SN-38 tECF exposure as compared to the irinotecan group, although SN-38 levels dropped below the quantifiable level after 21 h. In contrast, SN-38 levels were measurable for at least 24 h following administration of GD2-targeting 3F8-NPs in 3 out of 3 experiments; in 2 experiments, SN-38 was detectable beyond 48 h.

The calculated AUCs for plasma and tECF exposures to SN-38 are plotted in Figure 6C. Plasma exposure to unbound SN-38 upon administration of NPs was significantly lower than after equimolar irinotecan. The extent of penetration of the tumor by unbound SN-38, calculated as the mean tECF-to-plasma AUC ratio, was significantly higher in mice receiving 3F8-NPs, as compared to the other two groups (Figure 6D).

In vivo antitumor activity

Finally, we evaluated the anti-tumor activity of the nano-drug delivery systems administered i.v. (q3d)x3, when compared to equimolar irinotecan (same schedule), or one cycle of the published protracted regimen of irinotecan (dx5)x2 [4], in mice bearing the PDX models HSJD-NB-007 (GD2-high) and HSJD-NB-011 (GD2-low) (Figure 7A). Responses at the end of treatment are shown in Table 2. In the GD2-high model all animals receiving NPs achieved response to treatment, in contrast to the other 3 groups. Of note, 75% of animals treated with 3F8-NPs achieved CR. In the GD2-low model, only protracted irinotecan achieved response (100% CR) as compared to the modest effect achieved by the (q3d)x3 regimes, including the targeted NPs.

After the cessation of treatments, all tumors progressed in both models until endpoint (Figure 7B). In the GD2-high model (HSJD-NB-007), after Bonferroni correction for multiple comparisons of the median survivals (Table 2), P value threshold < 0.0071 was considered significant. Both NP-treated groups survived significantly longer than the control mice (P = 0.0064), whilst irinotecan 10 mg/kg at (q3d)x3 and (dx5)x2 schedules did not (P = 0.657 and P = 0.0181). Moreover, 3F8-NPs-treated mice survived significantly longer than mice treated with irinotecan (dx5)x2 (P = 0.0067), while IgG3-NPs-treated mice did not (P = 0.2647). Survival of 3F8-NPs-treated mice was also longer than that of IgG3-NPs-mice (P = 0.0409).

In the GD2-low model (NSJD-NB-011), only the animals receiving irinotecan 10 mg/kg (dx5)x2 achieved significant survival benefit as compared to the control group (P = 0.0004) (Table 2). In this model, NP treatment did not outperform equimolar irinotecan treatment. Survival of animals treated with 3F8-NPs and IgG3-NPs was similar (P = 0.8204).

Treatments were well tolerated by the animals, as shown by their weight curves (Figure 7C).

Discussion

The ability to maximize the concentration of the chemotherapeutic agent inside the tumor while reducing systemic exposure is one of the expected benefits of targeted nanomedicine [46]. However, the proper characterization of the distribution and fate of drug released from the targeted NPs can be challenging, since it will be a mixture of encapsulated and released drug in plasma, tumors, and other tissues [47]. We addressed this complex system by applying (i) microdialysis sampling to assess intratumoral pharmacokinetics of the released drug in living animals (thus eliminating the unreleased NPs-bound drug fraction from the analysis), and (ii) plasma ultrafiltration to differentiate between the encapsulated and the released drug in plasma. As a result, we demonstrate that drug released from NPs targeting GD2 accumulate in the tECF of GD2-expressing neuroblastoma, leading to improved drug activity. The approach described here might advance the accuracy with which we characterize intratumor pharmacokinetics for targeted therapies. In addition, our results may be clinically relevant for the design of new targeted therapies in children with tumors expressing GD2, since the feasibility of clinical translation of PLGA NPs targeting other cancer antigens has been demonstrated [32].

In our study, encapsulation of SN-38 into polymer NPs took advantage of the low solubility of the drug to allow efficient encapsulation in the hydrophobic biodegradable polymers PLGA and PLA, as previously described [10]. The inclusion of hydrophilic PEG in the particle corona provided long circulation properties and allowed for the conjugation of amine groups of the targeting antibody. Neither the selection of amine groups in the targeting ligands nor the efficient control of conjugation numbers and surface densities is allowed by the EDC/NHS conjugation chemistry [48]. Thus, we characterized the efficiency of the chemical process and the stability of the conjugated antibody.

The average particle size below 300 nm achieved in our study is considered sufficient for the accumulation of NPs in tumors through extravasation [15]. The release kinetics of SN-38

from the NPs, with no burst effect, is highly desirable to ensure that most of the cargo is released once the NPs reach the tumor and not in the systemic circulation immediately after injection, where it could provoke systemic toxicity. We confirmed that the encapsulation did not affect the cytotoxicity of SN-38, as previously described for other SN-38-loaded NPs [49]. The stability of camptothecins in PLGA NPs is improved by the hydrolysis of the polymer that creates an acidic microenvironment to conserve the lactone (active chemical form), which can be hydrolyzed to a carboxylate (inactive) at pH 7.4 upon *in vitro* culture or *in vivo* i.v. injection [50]. Similar IC50 values between targeted and non-targeted NPs were expected because (i) long-term (72 h) exposures to the NP products during *in vitro* assays allowed complete release of the encapsulated drug and (ii) the density of attached antibodies in 3F8-NPs (7 per particle) was relatively low, hence their concentration in culture would be below the inherent antiproliferative activity previously reported for 3F8 in neuroblastoma (>1 μg/mL) [51]. Higher activity of free SN-38 as compared to NP products in PDX-derived cultures might be caused by the spheroid structures formed by these primary cells in culture, which would act as barrier for NP penetration *in vitro* [52].

GD2 overexpression has been previously reported in neuroblastoma cell lines [21] but our study is the first confirming expression in neuroblastoma PDX models. Our pharmacokinetic analysis suggested that GD2-targeted SN-38 was released slowly in the extracellular compartment of the tumor HSJD-NB-007 (GD2-high). Whether the NPs remained in the tECF or penetrated the intracellular compartment of the tumor could not be addressed with our experimental design. We did not analyze SN-38 from tumor homogenates in this study because such analysis would detect a combination of unreleased (in the NPs) and released drug in different tumor compartments (intracellular, extracellular, and vascular) [30]. In contrast, analysis of dialysates made possible the comparison of the distribution of free SN-38 in a single compartment (tECF) for the 3 groups (Figure 6B and 6C). The microdialysis approach has been previously reported to characterize tECF distribution of anticancer drugs released from liposomal formulations [53, 54]. To our knowledge, our study is the first using microdialysis to characterize the distribution of a drug released from a polymeric nanocarrier in the tECF and the first to report enhanced drug distribution in tECF provided by the targeting of a specific tumor antigen.

We expected a positive correlation between SN-38 distribution in tECF and improved anti-tumor activity in GD2-high neuroblastoma, because unbound drug concentrations in tECF correlated well with antitumor activity in previous microdialysis studies [55–57], and protracted exposure to the camptothecins irinotecan and topotecan improved antitumor response as compared to short high-dose exposure [4, 58–60]. Lower plasma exposure to unbound SN-38 upon administration of NPs has implications for bystander toxicity, since systemic exposure to SN-38 causes diarrhea and neutropenia [61]. Although toxicology was not addressed by our study, similar products loaded with docetaxel have proven safe in animals and humans [32].

Our study did not address particle extravasation experimentally. Published data showed higher accumulation of fluorescent silica or iron oxide GD2-targeted NPs in neuroblastoma xenografts as compared to control NPs [25, 27]. However, in these previous studies, reference NPs were not conjugated to control antibodies to rule out the nonspecific

accumulation of NPs. Our results in the GD2-low PDX model, showing similar activity of GD2-targeted NPs and control NPs, suggest that active targeting with 3F8-NPs was likely to be more critical than the EPR effect to achieve prolonged drug exposure in our neuroblastoma PDX models. Other authors have shown that tocopherol succinate-conjugated SN-38, loaded in non targeted PLA-PEG NPs (<100 nm), improved the activity of systemic irinotecan in neuroblastoma xenografts and accumulated in tumors due to the EPR effect [12].

Our results of improved anti-neuroblastoma activity conferred by GD2-targeted chemotherapy differed in scope from previous GD2-targeting reports in the field. The activity of doxorubicin-loaded GD2-targeted liposomes in neuroblastoma has been reported elsewhere [24, 62]. However, in these studies, the pharmacokinetics of radiolabeled liposomes was only measured in plasma and not in the tumors. Moreover, the absence of adequate controls *in vivo* (i.e., liposomes conjugated to unspecific antibodies) did not address the specificity of targeting. Hence the enhanced anticancer activity could result from nonspecific effect of EPR or nonspecific antibody interactions.

Conclusion

In summary, we have shown the improved pharmacokinetics of SN-38 delivery using an antibody against GD2 to target SN-38 loaded NPs into human tumors. The use of the microdialysis technique demonstrated unequivocally the prolonged exposure to the targeted drug in the interstitial fluid of GD2-expressing tumors and thus eliminated the interference of the unreleased drug found in the classical pharmacokinetic assays based on homogenates. We showed that this delivery system is antigen specific *in vitro* and *in vivo*, establishing a proof of concept that GD2 targeting of NPs using monoclonal antibodies could have clinical potential to enhance anti-tumor activity while reducing toxicity in innocent bystanders. With fine tuning of the conjugation method to improve immunoreactivity of the antibody and of the avidity of tumor binding, the clinical potential of this platform could be further enhanced.

Acknowledgments

AMC acknowledges funding from AECC Scientific Foundation, MINECO (SAF2011-22660 and PRI-AIBAR-2011-0977), Fundacion BBVA, European Union Seventh Framework Programme (FP7/2007-2013) under Marie Curie International Reintegration Grant (PIRG-08-GA-2010-276998) and ISCIII-FEDER (CP13/00189). AS thanks partial funding of RBNI. CL thanks Asociacion NEN. We thank the patients' families for the support. Thanks to Eva Rodriguez and Maria J Nagel for technical assistance.

References

1. Vassal G, Zwaan CM, Ashley D, Le Deley MC, Hargrave D, Blanc P, Adamson PC. New drugs for children and adolescents with cancer: the need for novel development pathways. Lancet Oncol. 2013; 14:e117–e124. [PubMed: 23434337]
2. Pui CH, Gajjar AJ, Kane JR, Qaddoumi IA, Pappo AS. Challenging issues in pediatric oncology. Nature reviews. Clinical oncology. 2011; 8:540–549.
3. Cheung NK, Dyer MA. Neuroblastoma: developmental biology, cancer genomics and immunotherapy. Nat Rev Cancer. 2013; 13:397–411. [PubMed: 23702928]

4. Thompson J, Zamboni WC, Cheshire PJ, Lutz L, Luo X, Li Y, Houghton JA, Stewart CF, Houghton PJ. Efficacy of systemic administration of irinotecan against neuroblastoma xenografts. Clin Cancer Res. 1997; 3:423–431. [PubMed: 9815701]
5. Vassal G, Terrier-Lacombe MJ, Bissery MC, Venuat AM, Gyergyay F, Benard J, Morizet J, Boland I, Ardouin P, Bressac-de-Paillerets B, Gouyette A. Therapeutic activity of CPT-11, a DNA-topoisomerase I inhibitor, against peripheral primitive neuroectodermal tumour and neuroblastoma xenografts. Br J Cancer. 1996; 74:537–545. [PubMed: 8761367]
6. Bagatell R, London WB, Wagner LM, Voss SD, Stewart CF, Maris JM, Kretschmar C, Cohn SL. Phase II Study of Irinotecan and Temozolomide in Children With Relapsed or Refractory Neuroblastoma: A Children's Oncology Group Study. J Clin Oncol. 2011; 29:208–213.
7. Xie M, Yang D, Wu M, Xue B, Yan B. Mouse liver and kidney carboxylesterase (M-LK) rapidly hydrolyzes antitumor prodrug irinotecan and the N-terminal three quarter sequence determines substrate selectivity. Drug Metab Dispos. 2003; 31:21–27. [PubMed: 12485949]
8. Slatter JG, Schaaf LJ, Sams JP, Feenstra KL, Johnson MG, Bombardt PA, Cathcart KS, Verburg MT, Pearson LK, Compton LD, Miller LL, Baker DS, Pesheck CV, Lord RS 3rd. Pharmacokinetics, metabolism, and excretion of irinotecan (CPT-11) following I.V. infusion of [(14)C]CPT-11 in cancer patients. Drug Metab Dispos. 2000; 28:423–433. [PubMed: 10725311]
9. Stewart CF, Zamboni WC, Crom WR, Houghton PJ. Disposition of irinotecan and SN-38 following oral and intravenous irinotecan dosing in mice. Cancer Chemother Pharmacol. 1997; 40:259–265. [PubMed: 9219511]
10. Bala V, Rao S, Boyd BJ, Prestidge CA. Prodrug and nanomedicine approaches for the delivery of the camptothecin analogue SN38. J Control Release. 2013; 172:48–61. [PubMed: 23928356]
11. Monterrubio C, Pascual-Pasto G, Cano F, Vila-Ubach M, Manzanares A, Schaiquevich P, Tornero JA, Sosnik A, Mora J, Carcaboso AM. SN-38-loaded nanofiber matrices for local control of pediatric solid tumors after subtotal resection surgery. Biomaterials. 2016; 79:69–78. [PubMed: 26695118]
12. Iyer R, Croucher JL, Chorny M, Mangino JL, Alferiev IS, Levy RJ, Kolla V, Brodeur GM. Nanoparticle delivery of an SN38 conjugate is more effective than irinotecan in a mouse model of neuroblastoma. Cancer Lett. 2015; 360:205–212. [PubMed: 25684664]
13. Pastorino F, Loi M, Sapra P, Becherini P, Cilli M, Emionite L, Ribatti D, Greenberger LM, Horak ID, Ponzoni M. Tumor regression and curability of preclinical neuroblastoma models by PEGylated SN38 (EZN-2208), a novel topoisomerase I inhibitor. Clin Cancer Res. 2010; 16:4809–4821. [PubMed: 20702613]
14. Matsumura Y. Preclinical and clinical studies of NK012, an SN-38-incorporating polymeric micelles, which is designed based on EPR effect. Adv Drug Deliv Rev. 2011; 63:184–192. [PubMed: 20561951]
15. Maeda H, Wu J, Sawa T, Matsumura Y, Hori K. Tumor vascular permeability and the EPR effect in macromolecular therapeutics: a review. J Control Release. 2000; 65:271–284. [PubMed: 10699287]
16. Suzuki M, Cheung NK. Disialoganglioside GD2 as a therapeutic target for human diseases. Expert Opin Ther Targets. 2015; 19:349–362. [PubMed: 25604432]
17. Mackall CL, Merchant MS, Fry TJ. Immune-based therapies for childhood cancer. Nature reviews. Clinical oncology. 2014; 11:693–703.
18. Lo Piccolo MS, Cheung NK, Cheung IY. GD2 synthase: a new molecular marker for detecting neuroblastoma. Cancer. 2001; 92:924–931. [PubMed: 11550167]
19. Dobrenkov K, Ostrovnaya I, Gu J, Cheung IY, Cheung NK. Oncotargets GD2 and GD3 are highly expressed in sarcomas of children, adolescents, and young adults. Pediatr Blood Cancer. 2016; 63:1780–1785. [PubMed: 27304202]
20. Lammie G, Cheung N, Gerald W, Rosenblum M, Cordoncardo C. Ganglioside gd(2) expression in the human nervous-system and in neuroblastomas - an immunohistochemical study. International journal of oncology. 1993; 3:909–915. [PubMed: 21573452]
21. Cheung NK, Saarinen UM, Neely JE, Landmeier B, Donovan D, Coccia PF. Monoclonal antibodies to a glycolipid antigen on human neuroblastoma cells. Cancer Res. 1985; 45:2642–2649. [PubMed: 2580625]

22. Yu AL, Gilman AL, Ozkaynak MF, London WB, Kreissman SG, Chen HX, Smith M, Anderson B, Villablanca JG, Matthay KK, Shimada H, Grupp SA, Seeger R, Reynolds CP, Buxton A, Reisfeld RA, Gillies SD, Cohn SL, Maris JM, Sondel PM. Anti-GD2 antibody with GM-CSF, interleukin-2, and isotretinoin for neuroblastoma. N Engl J Med. 2010; 363:1324–1334. [PubMed: 20879881]

23. Dobrenkov K, Cheung NK. GD2-targeted immunotherapy and radioimmunotherapy. Semin Oncol. 2014; 41:589–612. [PubMed: 25440605]

24. Pastorino F, Brignole C, Marimpietri D, Sapra P, Moase EH, Allen TM, Ponzoni M. Doxorubicin-loaded Fab' fragments of anti-disialoganglioside immunoliposomes selectively inhibit the growth and dissemination of human neuroblastoma in nude mice. Cancer Res. 2003; 63:86–92. [PubMed: 12517782]

25. Tivnan A, Orr WS, Gubala V, Nooney R, Williams DE, McDonagh C, Prenter S, Harvey H, Domingo-Fernandez R, Bray IM, Piskareva O, Ng CY, Lode HN, Davidoff AM, Stallings RL. Inhibition of neuroblastoma tumor growth by targeted delivery of microRNA-34a using anti-disialoganglioside GD2 coated nanoparticles. PLoS One. 2012; 7:e38129. [PubMed: 22662276]

26. Vavere AL, Butch ER, Dearling JL, Packard AB, Navid F, Shulkin BL, Barfield RC, Snyder SE. 64Cu-p-NH2-Bn-DOTA-hu14.18K322A, a PET radiotracer targeting neuroblastoma and melanoma. J Nucl Med. 2012; 53:1772–1778. [PubMed: 23064212]

27. Baiu DC, Artz NS, McElreath MR, Menapace BD, Hernando D, Reeder SB, Grüttner C, Otto M. High specificity targeting and detection of human neuroblastoma using multifunctional anti-GD2 iron-oxide nanoparticles. Nanomedicine. 2015; 10:2973–2988. [PubMed: 26420448]

28. Hidalgo M, Amant F, Biankin AV, Budinska E, Byrne AT, Caldas C, Clarke RB, de Jong S, Jonkers J, Maelandsmo GM, Roman-Roman S, Seoane J, Trusolino L, Villanueva A. Patient-derived xenograft models: an emerging platform for translational cancer research. Cancer discovery. 2014; 4:998–1013. [PubMed: 25185190]

29. Hare JI, Lammers T, Ashford MB, Puri S, Storm G, Barry ST. Challenges and strategies in anti-cancer nanomedicine development: An industry perspective. Advanced Drug Delivery Reviews. 2017; 108:25–38. [PubMed: 27137110]

30. Carcaboso AM, Elmeliegy MA, Shen J, Juel SJ, Zhang ZM, Calabrese C, Tracey L, Waters CM, Stewart CF. Tyrosine kinase inhibitor gefitinib enhances topotecan penetration of gliomas. Cancer Res. 2010; 70:4499–4508. [PubMed: 20460504]

31. Monterrubio C, Paco S, Vila-Ubach M, Rodriguez E, Glisoni R, Lavarino C, Schaiquevich P, Sosnik A, Mora J, Carcaboso AM. Combined Microdialysis-Tumor Homogenate Method for the Study of the Steady State Compartmental Distribution of a Hydrophobic Anticancer Drug in Patient-Derived Xenografts. Pharm Res. 2015; 32:2889–2900. [PubMed: 25773723]

32. Hrkach J, Von Hoff D, Mukkaram Ali M, Andrianova E, Auer J, Campbell T, De Witt D, Figa M, Figueiredo M, Horhota A, Low S, McDonnell K, Peeke E, Retnarajan B, Sabnis A, Schnipper E, Song JJ, Song YH, Summa J, Tompsett D, Troiano G, Van Geen Hoven T, Wright J, LoRusso P, Kantoff PW, Bander NH, Sweeney C, Farokhzad OC, Langer R, Zale S. Preclinical development and clinical translation of a PSMA-targeted docetaxel nanoparticle with a differentiated pharmacological profile. Science translational medicine. 2012; 4:128ra139.

33. Vega E, Egea MA, Calpena AC, Espina M, Garcia ML. Role of hydroxypropyl-beta-cyclodextrin on freeze-dried and gamma-irradiated PLGA and PLGA-PEG diblock copolymer nanospheres for ophthalmic flurbiprofen delivery. International journal of nanomedicine. 2012; 7:1357–1371. [PubMed: 22457594]

34. Betancourt T, Byrne JD, Sunaryo N, Crowder SW, Kadapakkam M, Patel S, Casciato S, Brannon-Peppas L. PEGylation strategies for active targeting of PLA/PLGA nanoparticles. J Biomed Mater Res A. 2009; 91:263–276. [PubMed: 18980197]

35. Grey HM, Hirst JW, Cohn M. A new mouse immunoglobulin: IgG3. The Journal of experimental medicine. 1971; 133:289–304. [PubMed: 5133863]

36. Pascual-Pasto G, Olaciregui NG, Vila-Ubach M, Paco S, Monterrubio C, Rodriguez E, Winter U, Batalla-Vilacis M, Catala J, Salvador H, Parareda A, Schaiquevich P, Sunol M, Mora J, Lavarino C, de Torres C, Chantada GL, Carcaboso AM. Preclinical platform of retinoblastoma xenografts recapitulating human disease and molecular markers of dissemination. Cancer Lett. 2016; 380:10–19. [PubMed: 27319373]

37. Roth M, Linkowski M, Tarim J, Piperdi S, Sowers R, Geller D, Gill J, Gorlick R. Ganglioside GD2 as a therapeutic target for antibody-mediated therapy in patients with osteosarcoma. Cancer. 2014; 120:548–554. [PubMed: 24166473]
38. Carcaboso AM, Bramuglia GF, Chantada GL, Fandino AC, Chiappetta DA, de Davila MT, Rubio MC, Abramson DH. Topotecan vitreous levels after periocular or intravenous delivery in rabbits: an alternative for retinoblastoma chemotherapy. Invest Ophthalmol Vis Sci. 2007; 48:3761–3767. [PubMed: 17652749]
39. Houghton PJ, Morton CL, Tucker C, Payne D, Favours E, Cole C, Gorlick R, Kolb EA, Zhang W, Lock R, Carol H, Tajbakhsh M, Reynolds CP, Maris JM, Courtright J, Keir ST, Friedman HS, Stopford C, Zeidner J, Wu J, Liu T, Billups CA, Khan J, Ansher S, Zhang J, Smith MA. The pediatric preclinical testing program: description of models and early testing results. Pediatr Blood Cancer. 2007; 49:928–940. [PubMed: 17066459]
40. Bhakta S, Seraji MS, Suib SL, Rusling JF. Antibody-like Biorecognition Sites for Proteins from Surface Imprinting on Nanoparticles. ACS Appl Mater Interfaces. 2015; 7:28197–28206. [PubMed: 26636440]
41. Tan YH, Liu M, Nolting B, Go JG, Gervay-Hague J, Liu GY. A nanoengineering approach for investigation and regulation of protein immobilization. ACS Nano. 2008; 2:2374–2384. [PubMed: 19206405]
42. Ahmed M, Cheung NK. Engineering anti-GD2 monoclonal antibodies for cancer immunotherapy. FEBS Lett. 2014; 588:288–297. [PubMed: 24295643]
43. Craddock JA, Lu A, Bear A, Pule M, Brenner MK, Rooney CM, Foster AE. Enhanced tumor trafficking of GD2 chimeric antigen receptor T cells by expression of the chemokine receptor CCR2b. J Immunother. 2010; 33:780–788. [PubMed: 20842059]
44. Prapa M, Caldrer S, Spano C, Bestagno M, Golinelli G, Grisendi G, Petrachi T, Conte P, Horwitz EM, Campana D, Paolucci P, Dominici M. A novel anti-GD2/4-1BB chimeric antigen receptor triggers neuroblastoma cell killing. Oncotarget. 2015; 6:24884–24894. [PubMed: 26298772]
45. DeRose YS, Wang G, Lin YC, Bernard PS, Buys SS, Ebbert MT, Factor R, Matsen C, Milash BA, Nelson E, Neumayer L, Randall RL, Stijleman IJ, Welm BE, Welm AL. Tumor grafts derived from women with breast cancer authentically reflect tumor pathology, growth, metastasis and disease outcomes. Nat Med. 2011; 17:1514–1520. [PubMed: 22019887]
46. Sosnik A, Carcaboso AM. Nanomedicines in the future of pediatric therapy. Adv Drug Deliv Rev. 2014; 73:140–161. [PubMed: 24819219]
47. Zamboni WC, Torchilin V, Patri AK, Hrkach J, Stern S, Lee R, Nel A, Panaro NJ, Grodzinski P. Best practices in cancer nanotechnology: perspective from NCI nanotechnology alliance. Clin Cancer Res. 2012; 18:3229–3241. [PubMed: 22669131]
48. Kamaly N, Xiao Z, Valencia PM, Radovic-Moreno AF, Farokhzad OC. Targeted polymeric therapeutic nanoparticles: design, development and clinical translation. Chemical Society reviews. 2012; 41:2971–3010. [PubMed: 22388185]
49. Koizumi F, Kitagawa M, Negishi T, Onda T, Matsumoto S, Hamaguchi T, Matsumura Y. Novel SN-38-incorporating polymeric micelles, NK012, eradicate vascular endothelial growth factor-secreting bulky tumors. Cancer Res. 2006; 66:10048–10056. [PubMed: 17047068]
50. Shenderova A, Burke TG, Schwendeman SP. The acidic microclimate in poly(lactide-co-glycolide) microspheres stabilizes camptothecins. Pharm Res. 1999; 16:241–248. [PubMed: 10100309]
51. Cheung N-KV, Guo H, Hu J, Tassev DV, Cheung IY. Humanizing murine IgG3 anti-GD2 antibody m3F8 substantially improves antibody-dependent cell-mediated cytotoxicity while retaining targeting in vivo. Oncoimmunology. 2012; 1:477–486. [PubMed: 22754766]
52. Priwitaningrum DL, Blonde JG, Sridhar A, van Baarlen J, Hennink WE, Storm G, Le Gac S, Prakash J. Tumor stroma-containing 3D spheroid arrays: A tool to study nanoparticle penetration. J Control Release. 2016; 244:257–268. [PubMed: 27616660]
53. Zamboni WC, Strychor S, Joseph E, Walsh DR, Zamboni BA, Parise RA, Tonda ME, Yu NY, Engbers C, Eiseman JL. Plasma, tumor, and tissue disposition of STEALTH liposomal CKD-602 (S-CKD602) and nonliposomal CKD-602 in mice bearing A375 human melanoma xenografts. Clin Cancer Res. 2007; 13:7217–7223. [PubMed: 18056203]

54. Zamboni WC, Gervais AC, Egorin MJ, Schellens JH, Zuhowski EG, Pluim D, Joseph E, Hamburger DR, Working PK, Colbern G, Tonda ME, Potter DM, Eiseman JL. Systemic and tumor disposition of platinum after administration of cisplatin or STEALTH liposomal-cisplatin formulations (SPI-077 and SPI-077 B103) in a preclinical tumor model of melanoma. Cancer Chemother Pharmacol. 2004; 53:329–336. [PubMed: 14673619]

55. Daryani VM, Patel YT, Tagen M, Turner DC, Carcaboso AM, Atkinson JM, Gajjar A, Gilbertson RJ, Wright KD, Stewart CF. Translational Pharmacokinetic-Pharmacodynamic Modeling and Simulation: Optimizing 5-Fluorouracil Dosing in Children With Pediatric Ependymoma. CPT Pharmacometrics Syst Pharmacol. Apr 14.2016

56. Atkinson JM, Shelat AA, Carcaboso AM, Kranenburg TA, Arnold LA, Boulos N, Wright K, Johnson RA, Poppleton H, Mohankumar KM, Feau C, Phoenix T, Gibson P, Zhu L, Tong Y, Eden C, Ellison DW, Priebe W, Koul D, Yung WK, Gajjar A, Stewart CF, Guy RK, Gilbertson RJ. An integrated in vitro and in vivo high-throughput screen identifies treatment leads for ependymoma. Cancer Cell. 2011; 20:384–399. [PubMed: 21907928]

57. Morfouace M, Shelat A, Jacus M, Freeman BB 3rd, Turner D, Robinson S, Zindy F, Wang YD, Finkelstein D, Ayrault O, Bihannic L, Puget S, Li XN, Olson JM, Robinson GW, Guy RK, Stewart CF, Gajjar A, Roussel MF. Pemetrexed and gemcitabine as combination therapy for the treatment of Group3 medulloblastoma. Cancer Cell. 2014; 25:516–529. [PubMed: 24684846]

58. Santana VM, Furman WL, Billups CA, Hoffer F, Davidoff AM, Houghton PJ, Stewart CF. Improved response in high-risk neuroblastoma with protracted topotecan administration using a pharmacokinetically guided dosing approach. J Clin Oncol. 2005; 23:4039–4047. [PubMed: 15961757]

59. Houghton PJ, Cheshire PJ, Hallman JD, Lutz L, Friedman HS, Danks MK, Houghton JA. Efficacy of topoisomerase I inhibitors, topotecan and irinotecan, administered at low dose levels in protracted schedules to mice bearing xenografts of human tumors. Cancer Chemother.Pharmacol. 1995; 36:393–403. [PubMed: 7634381]

60. Furman WL, Stewart CF, Poquette CA, Pratt CB, Santana VM, Zamboni WC, Bowman LC, Ma MK, Hoffer FA, Meyer WH, Pappo AS, Walter AW, Houghton PJ. Direct translation of a protracted irinotecan schedule from a xenograft model to a phase I trial in children. J Clin Oncol. 1999; 17:1815–1824. [PubMed: 10561220]

61. Nagano T, Yasunaga M, Goto K, Kenmotsu H, Koga Y, Kuroda J, Nishimura Y, Sugino T, Nishiwaki Y, Matsumura Y. Antitumor activity of NK012 combined with cisplatin against small cell lung cancer and intestinal mucosal changes in tumor-bearing mouse after treatment. Clin Cancer Res. 2009; 15:4348–4355. [PubMed: 19509138]

62. Brignole C, Marimpietri D, Gambini C, Allen TM, Ponzoni M, Pastorino F. Development of Fab′ fragments of anti-GD2 immunoliposomes entrapping doxorubicin for experimental therapy of human neuroblastoma. Cancer Letters. 2003; 197:199–204. [PubMed: 12880982]

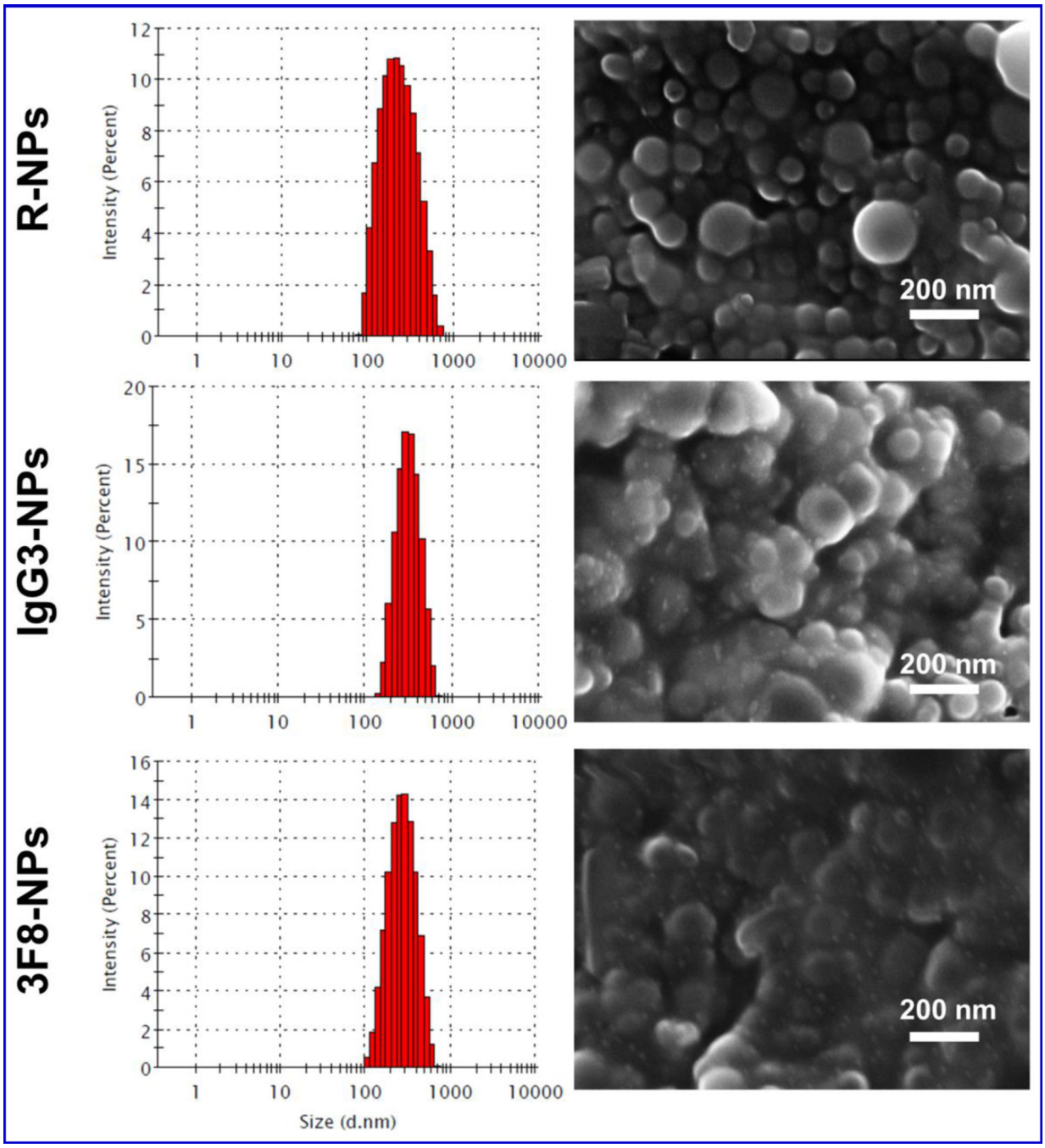

Figure 1.
Characterization of the SN-38-loaded unmodified and antibody-modified NPs, as determined by DLS and HR-SEM.

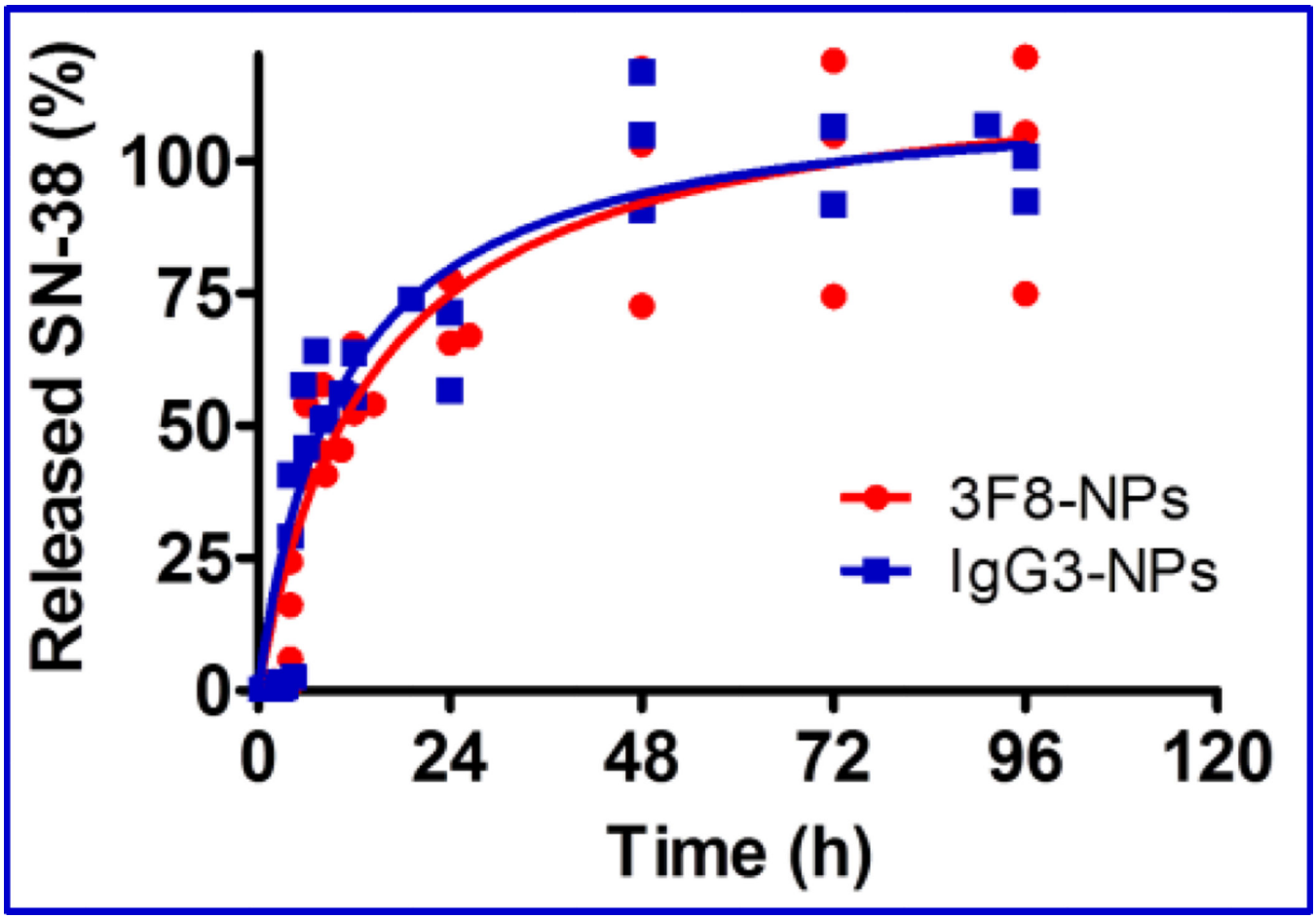

Figure 2.
Cumulative release of SN-38 from IgG3-NPs and 3F8-NPs. Dots are individual data at each sampling time, obtained from triplicate samples of each formulation.

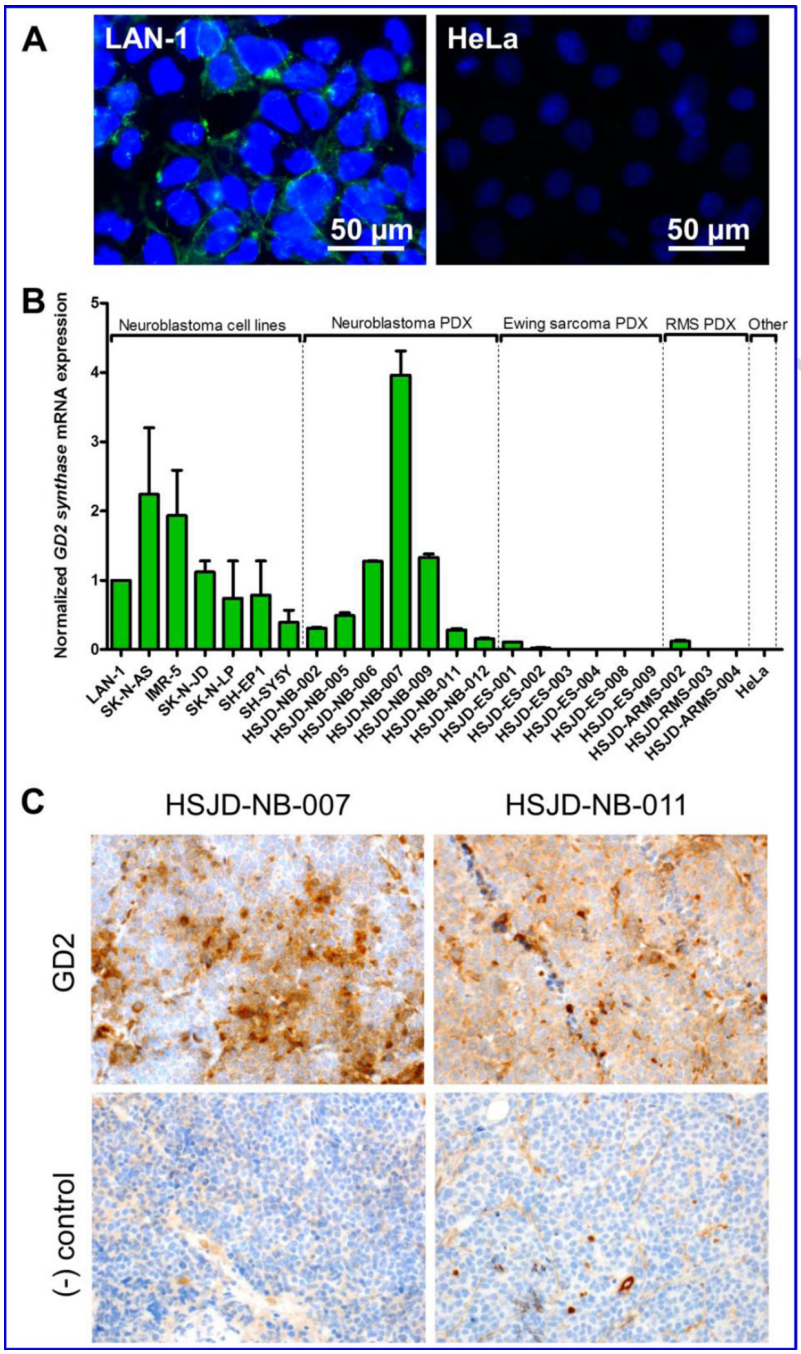

Figure 3.

Expression of GD2 in tumor models. (A) Immunocytochemistry of a GD2(+) neuroblastoma, LAN-1, and a GD2(−) model, HeLa. Green: GD2 staining by 3F8 antibody; Blue: nuclear DAPI staining. (B) Relative expression of *GD2 synthase* in neuroblastoma cell lines and PDX models of neuroblastoma, Ewing sarcoma (all of them EWS-FLI1 fusion-positive) and rhabdomyosarcoma (RMS; including two PAX3-FKHR fusion-positive alveolar rhabdomyosarcomas, ARMS). Values (mean and SD from triplicates) were normalized to *GD2 synthase* expression in LAN-1 cells. PDX models named with the suffix

HSJD were developed from patient biopsies or autopsies under an IRB-aproved protocol. (C) GD2 staining in neuroblastoma PDX models. Primary antibody was 3F8. Negative controls (tissue slides incubated with no primary antibody) are shown for comparison.

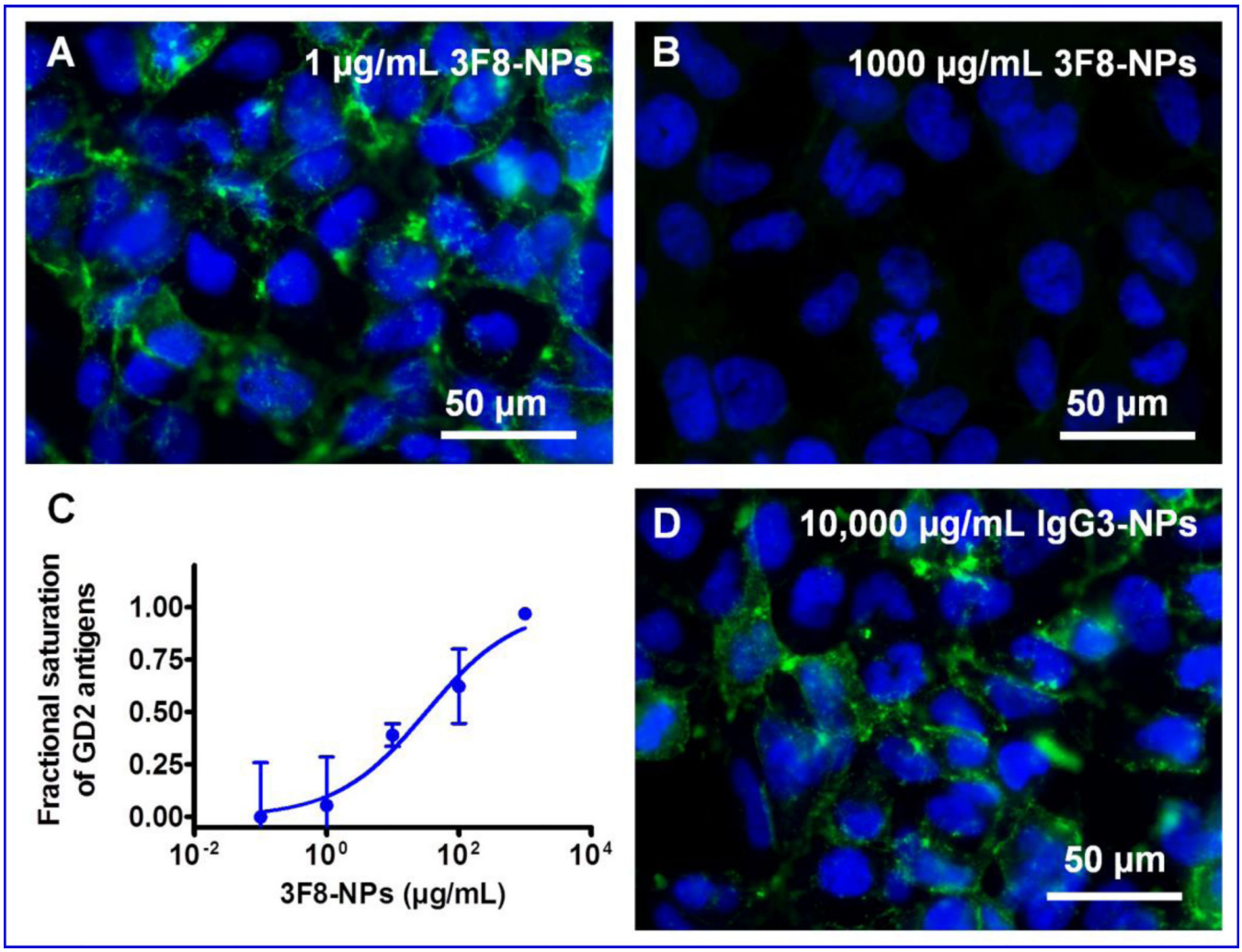

Figure 4.

Competitive immunofluorescence assay. (A) GD2 labeling by free 3F8 in LAN-1 cells exposed to 1 μg/mL of 3F8-NPs. This concentration of NPs did not saturate the GD2 antigens in the plate. (B) GD2 labeling in LAN-1 cells exposed to 1000 μg/mL of 3F8-NPs. This concentration of NPs blocked the subsequent binding of free 3F8 antibody. (C) Dose-response curve of the saturation of GD2 antigens exposed to increasing concentrations of 3F8-NPs. (D) IgG3-NPs at high concentration (10,000 μg/mL) did not compete with 3F8 for GD2 sites in LAN-1 cells. Green: GD2 staining by 3F8; blue: DAPI staining.

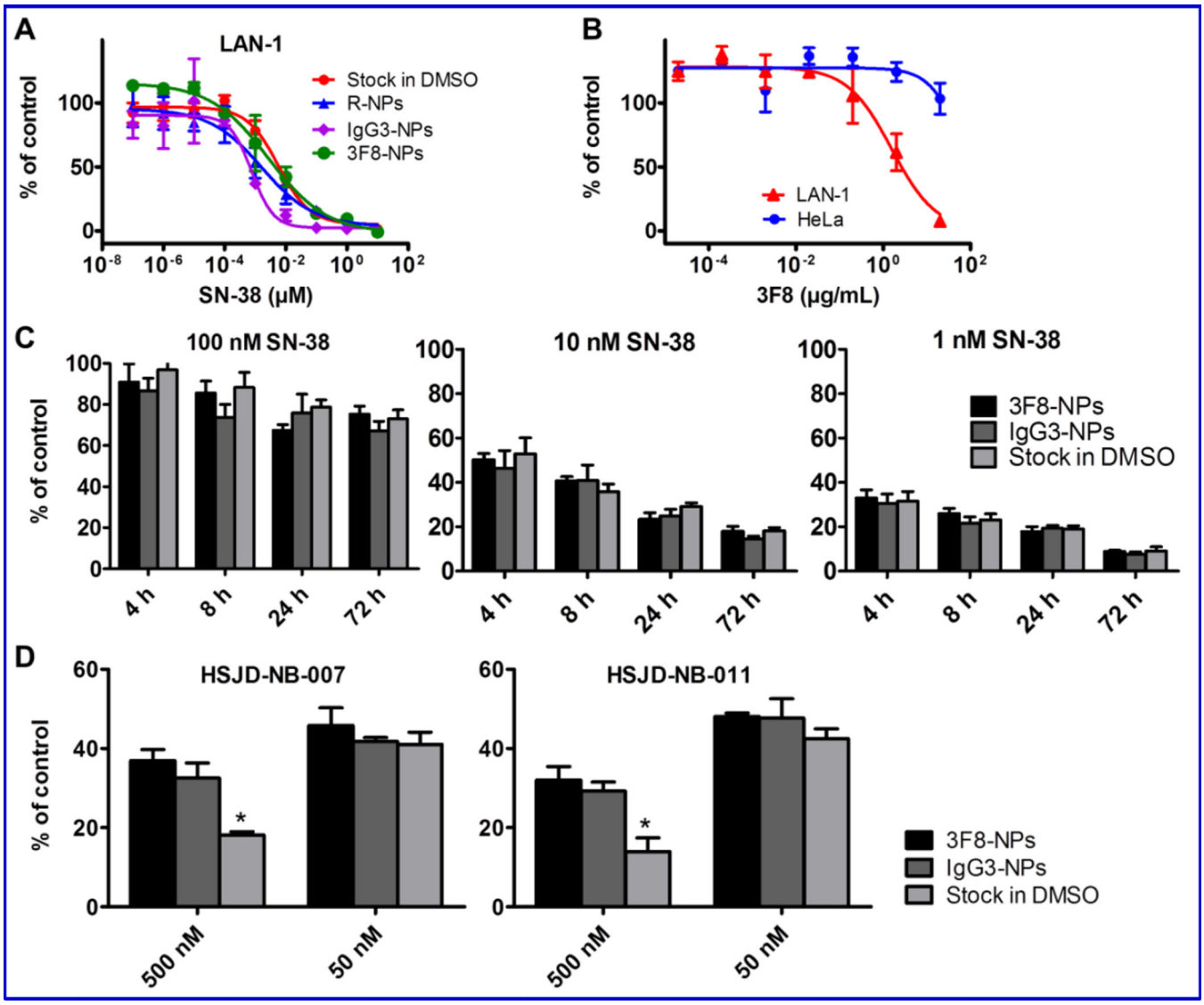

Figure 5.

In vitro antiproliferative activity of the NP products, SN-38 and 3F8 against LAN-1 and HeLa cell lines and primary cultures HSJD-NB-007 and HSJD-NB-011. (A) Activity of SN-38-loaded NPs in LAN-1. (B) Activity of free 3F8 antibody in LAN-1 and HeLa. (C) Time-course response of LAN-1 to SN-38 products at concentrations 100, 10 and 1 nM. (D) Activity of SN-38-loaded NPs in primary cultures derived from xenografts at concentrations 500 and 50 nM. Values are expressed as % of the MTS assay signal (mean and SD of 3–6 values) as compared to control untreated cells that were considered 100%. *P < 0.05; ANOVA.

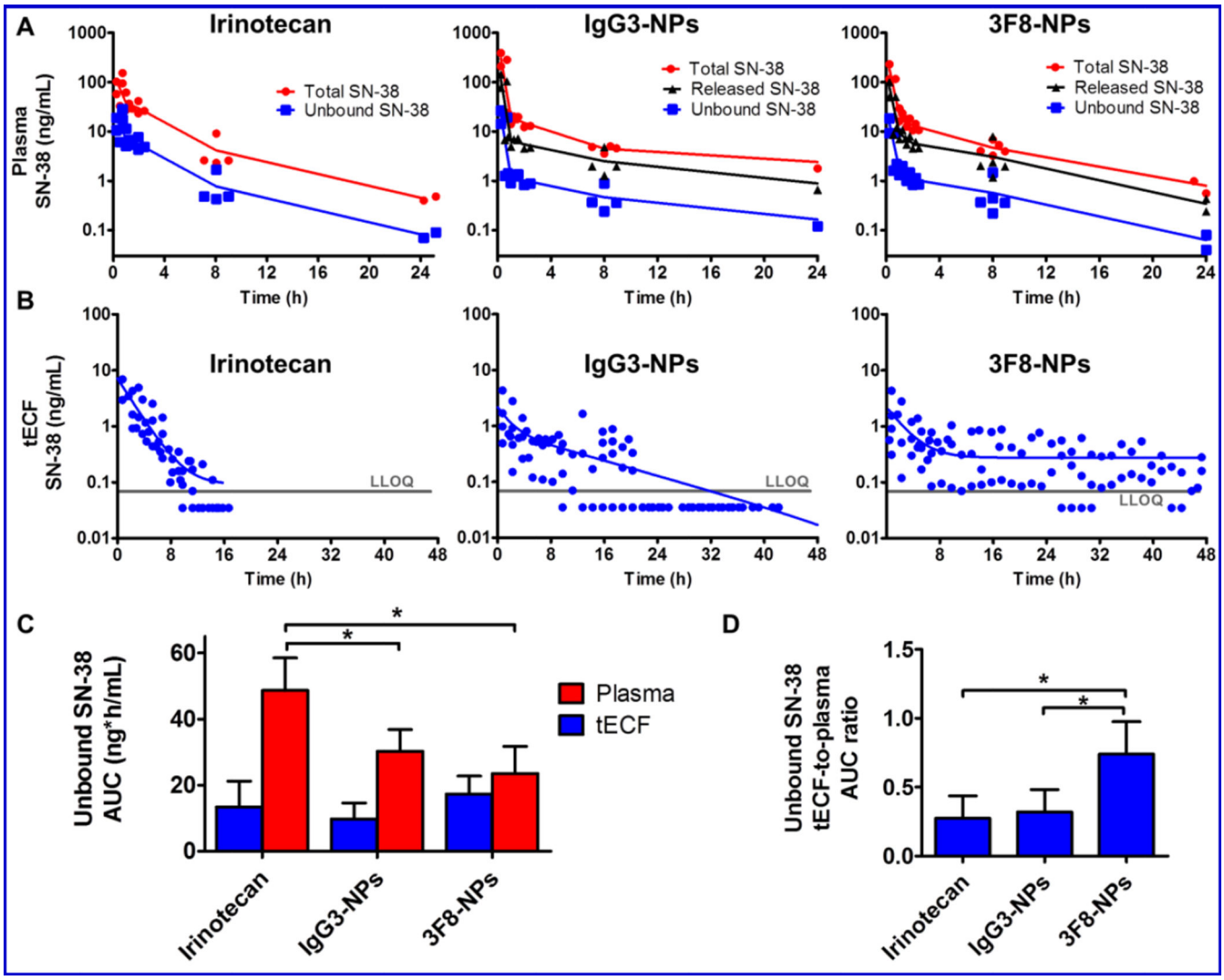

Figure 6.

Plasma and tECF pharmacokinetics of SN-38. (A) Plasma SN-38 concentration-time curves. Dots represent individual data and lines connect the average at each time point. A maximum of 3 blood samples were obtained from each mouse. (B) tECF SN-38 concentration-time curves. Dots represent individual data from 3–5 pooled experiments. Grey line: Lower limit of quantification (LLOQ; 0.07 ng/mL). Samples in which SN-38 was not quantifiable (below LLOQ) are represented as LLOQ/2 in the plots. (C) Plasma and tECF exposure to unbound SN-38, represented as calculated AUCs and SD. (D) tECF-to-plasma AUC ratios. Mean and SD of 3–5 experiments are represented. * $P < 0.05$ (ANOVA).

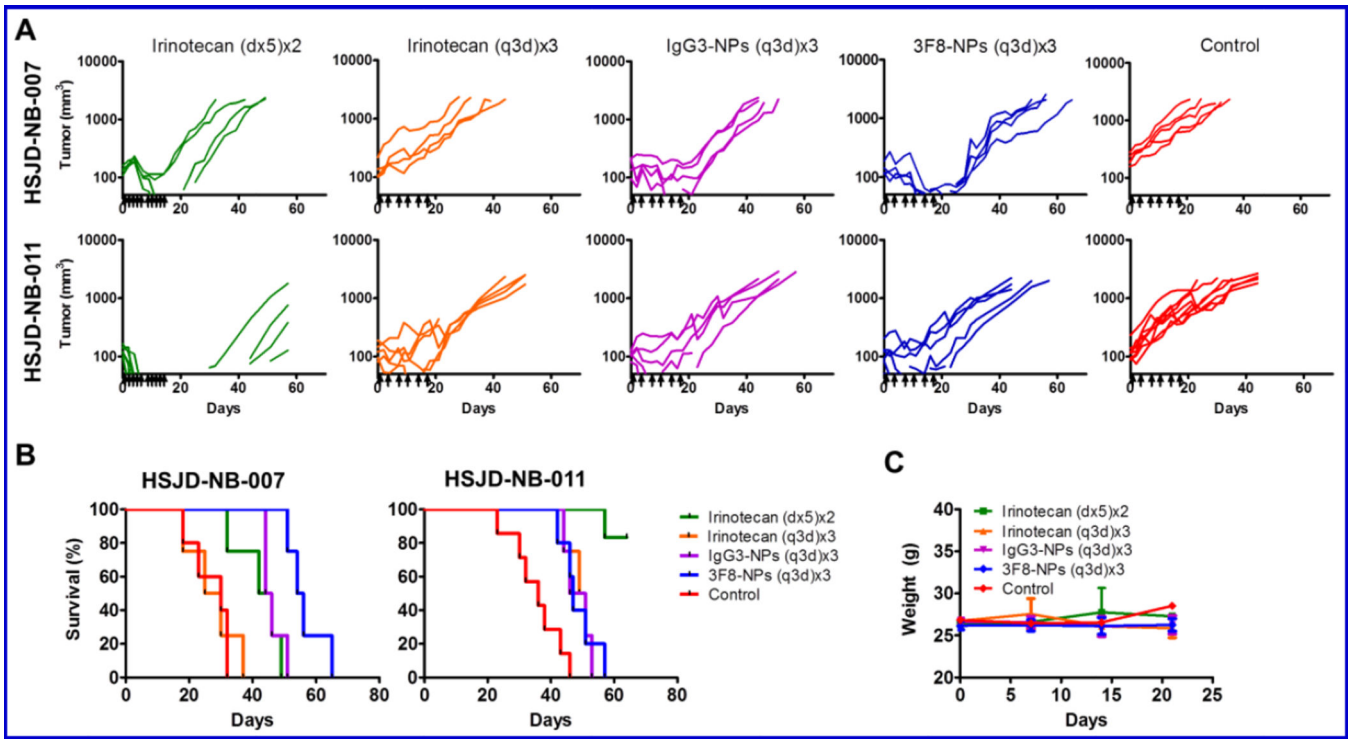

Figure 7.

In vivo efficacy of SN-38 formulations in PDX models HSJD-NB-007 (GD2-high) and HSJD-NB-011 (GD2-low). A. Antitumor activity of irinotecan 10 mg/kg (dx5)x2, irinotecan 10 mg/kg (q3d)x3, IgG3-NPs and 3F8-NPs at dosages equimolar to irinotecan 10 mg/kg (q3d)x3, as compared to control (saline-treated) mice. Graphs show growth of individual tumors in nude mice. Arrows indicate dosing times. B. Survival Kaplan-Meier curves. C. Weight of mice during treatment (mean and SD).

Table 1

Characterization of the NP products. Data are means of 3–4 different batches.

Product	mAb	Load efficiency (%) ± SD	Particle size (nm) ± SD	PDI ± SD	Zeta-potential (mV) ± SD	NP count per mg ± SD	Antibody count per NP ± SD
R-NPs	N/A	113.5 ± 7.8	276 ± 1	0.277 ± 0.025	−26.4 ± 1.55	Not done	N/A
IgG3-NPs	IgG3	83.1 ± 17.4	269 ± 5	0.259 ± 0.036	−20.0 ± 1.37	5.8E+11 ± 9.7E+09	Not done
3F8-NPs	3F8	90.7 ± 17.7	272 ± 19	0.282 ± 0.015	−22.8 ± 1.04	5.4E+11 ± 2.9E+10	7.19 ± 0.22

N/A: Not applicable.

Table 2

Response at the end of treatment[a] and median survivals.

Tumor model	Treatment	Mice (N)	PD (%)	SD (%)	PR (%)	CR (%)	Survival (days)
HSJD-NB-007 (GD2-high)	Control	5	100	0	0	0	30
	Irinotecan (dx5)x2	4	50	0	0	50	44
	Irinotecan (q3d)x3	4	100	0	0	0	28
	IgG3-NPs	4	0	100	0	0	45
	3F8-NPs	4	0	25	0	75	55
HSJD-NB-011 (GD2-low)	Control	8	100	0	0	0	36
	Irinotecan (dx5)x2	7	0	0	0	100	>64
	Irinotecan (q3d)x3	5	80	20	0	0	50
	IgG3-NPs	5	60	40	0	0	49
	3F8-NPs	6	50	50	0	0	47

[a]End of treatment was day 14 for the irinotecan (dx5)x2 group, and day 21 for the remaining groups.

PD: progressive disease; SD: stable disease; PR: partial response; CR: complete response.